Journal of Organometallic Chemistry, 325 (1987) 271–283
Elsevier Sequoia S.A., Lausanne – Printed in The Netherlands

CHEMISTRY OF PLATINUM-SULPHIDO COMPLEXES

VII *. REACTIONS OF $[Pt_2(\mu\text{-}S)(CO)(PPh_3)_3]$ WITH GROUP IB METAL IONS **

MALCOLM F. HALLAM, MICHAEL A. LUKE, D. MICHAEL P. MINGOS* and IAN D. WILLIAMS
Inorganic Chemistry Laboratory, University of Oxford, South Parks Road, Oxford OX1 3QR (Great Britain)
(Received October 24th, 1986)

Summary

The lone pair of the μ_2-sulphido ligand in the platinum–platinum bonded dimer $[Pt_2(\mu\text{-}S)(CO)(PPh_3)_3]$ (**1**) is sufficiently nucleophilic to form complexes with Group IB metal ions of the following types: $[Pt_2M(\mu_3\text{-}S)(CO)(PPh_3)_4](PF_6)$ (M = Cu (**2a**); Ag (**2b**) and Au (**2c**)) and $[\{Pt_2(\mu_3\text{-}S)(CO)(PPh_3)_3\}_2Au](PF_6)$ (**3**). The compounds have been characterised by infrared, $^{31}P\{^1H\}$ and $^{195}Pt\{^1H\}$ NMR spectroscopy and in the case of **2c** a single crystal X-ray crystallographic determination. The Pt–Pt and Pt–Au distances in **2c** clearly demonstrate that the metal–metal bond remains localised between the platinum atoms and only weak bonds are formed between the platinum and gold atoms.

In previous papers in this series [1] the ability of $[Pt_2S_2(PPh_3)_4]$ to function as a ligand through the sulphur atoms to a wide range of metal ions was reported. The resulting complexes were described as 'aggregates' rather than clusters because the metal–metal separations are all 3.0–3.3 Å and are therefore outside the range generally associated with metal–metal bonds with a formal bond order of one. The catalytic properties of some of these compounds have also been investigated [1]. As an extension of this work it was of interest to establish whether the related complex $[Pt_2(\mu_2\text{-}S)(CO)(PPh_3)_3]$ (**1**), first synthesised by Baird and Wilkinson [2–5] was also sufficiently nucleophilic to function as a ligand through the bridging sulphido ligand towards other metal ions. In **1** the platinum atoms are joined by a bond of length 2.65 Å [4], which raises the interesting question of whether this bond remains localised between the platinum atoms (I) or becomes delocalised (II) when it coordinates to a metal atom M. In order to maximise the possibilities for the

* For part VI see ref. 1.
** Dedicated to Professor G.E. Coates on the occasion of his 70th birthday.

0022-328X/87/$03.50

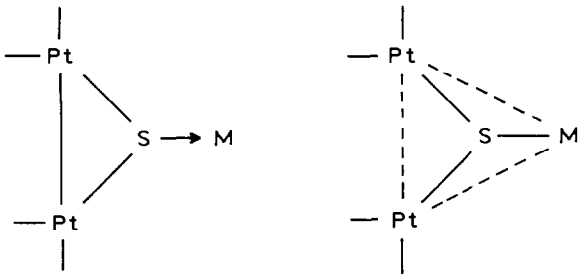

(I) (II)

formation of delocalised metal–metal bonds with a fractional bond order the complexes formed between **1** and Group IB metal ions were studied.

The compounds $[Pt_2M(\mu_2\text{-}S)(CO)(PPh_3)_4](PF_6)$ (M = Cu (**2a**); M = Ag (**2b**) and M = Au (**2c**)) were formed when solutions of **1** in THF were reacted with $[M(PPh_3)]^+$ formed in situ from $[MCl(PPh_3)]_m$ in $TlPF_6$ in THF. When the mole ratio is kept to 1/1 the compounds are formed in high yield ($\geq$ 80%) as yellow crystalline compounds. Coordination of the metal ions to sulphur results in a small shift to higher frequencies of ν(CO) compared to **1** (ν(CO) Nujol 2001 cm^{-1}); **2a** 2016, **2b** 2022 and **2c** 2025 cm^{-1}. The coordination of two molecules of **1** to Au^+ was achieved by mixing **1** and $[AuCl(Me_2S)]$ in a 2/1 mole ratio in benzene in the presence of an excess of $TlPF_6$. The resulting $[\{Pt_2(\mu_3\text{-}S)(CO)(PPh_3)_3\}_2Au](PF_6)$ salt was obtained in 72% yield as an orange solid and has two ν(CO) stretching modes at 2031 and 2019 cm^{-1} (Nujol).

The structure of the salts was confirmed by a single crystal X-ray crystallographic analysis on **2c**. The details of the data collection are summarised in Table 1, positional and thermal parameters in Table 2 and important bond lengths and angles in Table 3. The inner coordination sphere of the $[Pt_2Au(\mu_3\text{-}S)(CO)(PPh_3)_4]^+$ cation is illustrated in Fig. 1. The three metal atoms in **2c** define a distorted triangle. The Pt–Pt distance is not significantly different from that found in the parent compound **1**, 2.649(2) vs. 2.647(2) Å. The gold atom is not located equidistant from

TABLE 1

SUMMARY OF SINGLE CRYSTAL X-RAY DATA FOR $[Pt_2S(CO)(PPh_3)_3Au(PPh_3)](PF_6)\cdot CH_2Cl_2$

$C_{73}H_{60}AuF_6OP_5Pt_2S\cdot CH_2Cl_2$ $M = 1926.2$
Triclinic, space group $P\bar{1}$, $Z = 2$
a 11.065(22) Å
b 13.903(13) Å
c 26.439(13) Å
α 89.81(6)°
β 79.31(8)°
γ 79.00(12)°
U 3921 $Å^3$
D_c 1.63 g cm^{-3}
Final $R = 0.079$
Crystal dimensions 0.1 × 0.05 × 0.1 mm
μ(Mo-K_α) 57.06 cm^{-1}

TABLE 2

FINAL FRACTIONAL ATOMIC COORDINATES AND ISOTROPIC TEMPERATURE FACTORS ($Å^2$) FOR $[Pt_2(\mu\text{-}S)(CO)(PPh_3)_3Au(PPh_3)]PF_6$ (with estimated standard deviations in parentheses)

Atom	x/a	y/b	z/c	U_{iso} ($\times 10^4$)
Pt(1)	1852(1)	4772(1)	2842.3(6)	429
Pt(2)	1700(1)	5122(1)	1868.3(6)	410
Au(1)	−89(1)	6722(1)	2544.9(7)	570
S(1)	29(8)	5032(7)	2517(4)	365
P(1)	−272(12)	8385(9)	2545(5)	787
P(2)	891(9)	5227(7)	1110(4)	443
P(3)	1110(9)	4778(8)	3704(4)	490
P(4)	3970(9)	4378(8)	2773(4)	525
P(5)	5000	0	10000	1203(77)
F(51)	3640(43)	10061(33)	273(18)	2032(173)
F(52)	4678(66)	924(50)	9766(28)	3020(297)
F(53)	5196(57)	439(47)	479(24)	2716(256)
O(1)	4275(30)	5353(21)	1380(12)	882(92)
Cl(2)	971(47)	9548(40)	61(22)	4184(265)
Cl(3)	4631(65)	9386(51)	4491(26)	767(134)
C(1)	3297(44)	5259(31)	1556(17)	767(134)
C(2)	334(75)	458(56)	9510(32)	641(234)
C(3)	4164(101)	528(81)	4991(14)	1144(357)
C(110)	962(45)	8727(48)	2088(17)	1260(117)
C(111)	2035(66)	8001(32)	1956(24)	2124(148)
C(112)	3086(44)	8207(55)	1630(27)	2622(194)
C(113)	3065(56)	9140(67)	1435(21)	2239(224)
C(114)	1992(79)	9866(42)	1567(25)	2622(194)
C(115)	940(53)	9659(39)	1894(24)	2124(148)
C(120)	−306(61)	8853(33)	3181(17)	1260(117)
C(121)	750(44)	9146(40)	3298(26)	2124(148)
C(122)	733(63)	9465(43)	3800(32)	2622(194)
C(123)	−341(89)	9492(44)	4186(20)	2239(224)
C(124)	−1396(63)	9199(46)	4069(23)	2622(194)
C(125)	−1379(43)	8880(40)	3567(28)	2124(148)
C(130)	−1600(39)	8901(42)	2260(21)	1260(117)
C(131)	−2086(60)	8504(36)	1863(21)	2124(148)
C(132)	−3117(67)	9044(61)	1689(19)	2622(194)
C(133)	−3662(46)	9982(57)	1913(29)	2239(224)
C(134)	−3176(60)	10379(35)	2310(28)	2622(194)
C(135)	−2145(63)	9839(46)	2484(17)	2124(148)
C(210)	1921(25)	5718(23)	584(11)	674(123)
C(211)	2243(31)	6616(22)	676(11)	1033(166)
C(212)	3118(32)	6983(18)	322(14)	1006(163)
C(213)	3672(27)	6442(24)	−125(12)	1073(173)
C(214)	3361(29)	5550(23)	−218(10)	900(150)
C(215)	2487(28)	5178(17)	135(21)	747(131)
C(220)	−644(18)	5896(18)	1110(10)	556(110)
C(221)	−1643(25)	5682(19)	1473(9)	621(117)
C(222)	−2879(21)	6125(21)	1443(10)	752(131)
C(223)	−3102(20)	6776(22)	1055(12)	918(152)
C(224)	−2104(28)	6988(20)	698(10)	1092(176)
C(225)	−871(23)	6551(20)	724(9)	594(114)
C(230)	842(28)	3985(17)	900(11)	625(118)
C(231)	−175(23)	3742(20)	722(12)	732(130)

continued

TABLE 2 (continued)

Atom	x/a	y/b	z/c	U_{iso} ($\times 10^4$)
C(232)	−157(27)	2783(24)	562(12)	959(157)
C(233)	882(34)	2051(17)	579(13)	1032(167)
C(234)	1906(27)	2281(20)	756(14)	1132(180)
C(235)	1886(24)	3243(24)	916(12)	902(150)
C(310)	1137(29)	3608(17)	4018(12)	635(118)
C(311)	278(26)	3495(22)	4464(13)	1046(170)
C(312)	367(30)	2590(27)	4701(11)	1330(211)
C(313)	1305(34)	1808(20)	4499(13)	929(152)
C(314)	2161(28)	1913(19)	4058(13)	1105(176)
C(315)	2080(26)	2812(23)	3816(10)	756(131)
C(320)	−553(22)	5395(24)	3897(12)	712(127)
C(321)	−896(34)	6292(24)	4171(13)	1136(181)
C(322)	−2152(39)	6722(21)	4315(14)	1433(227)
C(323)	−3047(25)	6245(27)	4183(15)	1311(206)
C(324)	−2719(26)	5353(26)	3913(14)	1057(170)
C(325)	−1456(31)	4921(19)	3766(11)	678(123)
C(330)	1870(25)	5494(20)	4094(11)	540(109)
C(331)	2219(28)	6342(21)	3975(9)	789(136)
C(332)	2902(30)	6877(18)	4120(13)	939(156)
C(333)	3237(30)	6565(24)	4585(13)	1169(186)
C(334)	2894(31)	5726(25)	4803(10)	968(157)
C(335)	2212(28)	5190(18)	4559(11)	831(141)
C(410)	4681(25)	3620(19)	3236(9)	556(110)
C(411)	4732(26)	4089(15)	3695(12)	705(125)
C(412)	5095(30)	3559(24)	4106(9)	899(150)
C(413)	5412(31)	2548(24)	4056(10)	1337(112)
C(414)	5364(28)	2077(15)	3598(12)	775(134)
C(415)	4997(26)	2610(19)	3183(9)	633(118)
C(420)	4720(28)	3579(20)	2175(10)	615(116)
C(421)	5892(27)	3615(21)	1888(13)	951(156)
C(422)	6396(23)	2987(26)	1466(12)	1011(163)
C(423)	5718(32)	2325(23)	1328(11)	1185(188)
C(424)	4549(31)	2278(20)	1605(13)	908(150)
C(425)	4053(22)	2912(22)	2030(11)	731(129)
C(430)	4770(26)	5392(17)	2710(11)	627(117)
C(431)	4068(21)	6290(22)	2632(12)	678(123)
C(432)	4554(29)	7147(16)	2648(13)	1032(166)
C(433)	5763(31)	7087(18)	2740(13)	964(158)
C(434)	6463(22)	6185(24)	2818(13)	906(151)
C(435)	5974(24)	5340(17)	2804(11)	645(120)

the two platinum atoms, but the length of the bond to the platinum bearing the CO ligand is significantly shorter, 3.016(2) vs. 3.312(2) Å. The latter is well out of the range normally associated with platinum–gold bonds [6–8], but the former is just on the limit of those distances which have been associated with metal–metal bonding in clusters, and those molecules where weak gold–gold interactions have been invoked. For example, the average gold–gold distance in $[(Ph_3PAu)_2S]PF_6$ is 3.175 Å [9,10].

The Pt–S–Au bond angles of 91.3(3) and 81.3(3)° are similar to those reported for $[(Ph_3PAu)_3S](PF_6)$ (82.8–94.9°) and the Au–S distance of 2.33(1) Å lies in the range anticipated for this bond. Whether the observed distortion of the gold atom towards the platinum bearing the CO could arise from either steric or electronic

TABLE 3

SELECTED MOLECULAR DIMENSIONS FOR $[Pt_2(\mu\text{-}S)(CO)(PPh_3)_3Au(PPh_3)]^+ PF_6^-$ (estimated standard deviations in parentheses)

Intramolecular distances (Å)	
Pt(1)–Au	3.312(2)
Pt(2)–Au	3.016(2)
Pt(1)–Pt(2)	2.649(2)
Pt(1)–S	2.301(8)
Pt(2)–S	2.302(9)
Au–S	2.329(9)
Pt(1)–P(3)	2.27(1)
Pt(1)–P(4)	2.28(1)
Pt(2)–P(2)	2.34(1)
Pt(2)–C(1)	1.87(5)
Au–P(1)	2.28(1)
C(1)–O	1.11(4)
Bond angles (°)	
Pt(1)–S–Pt(2)	70.3(2)
Au–S–Pt(1)	91.3(3)
Au–S–Pt(2)	81.3(3)
S–Pt(1)–Pt(2)	54.9(2)
S–Pt(1)–P(3)	101.8(3)
S–Pt(1)–P(4)	153.8(4)
P(3)–Pt(1)–Pt(2)	155.4(3)
P(4)–Pt(1)–Pt(2)	100.1(3)
P(4)–Pt(1)–P(3)	103.9(4)
S–Pt(2)–Pt(1)	54.9(2)
S–Pt(2)–P(2)	105.5(3)
P(2)–Pt(2)–Pt(1)	159.2(2)
C(1)–Pt(2)–Pt(1)	105.2(13)
C(1)–Pt(2)–P(2)	94.9(14)
C(1)–Pt(1)–S	159.2(15)
S–Au–P(1)	177.3(4)

factors is uncertain and in the absence of additional data must remain an open question.

$^{31}P\{^1H\}$ and $^{195}Pt\{^1H\}$ NMR studies

Balch et al. carried out an analysis of the $^{31}P\{^1H\}$ NMR spectrum of $[Pt_2(\mu\text{-}S)(CO)(PPh_3)_3]$ involving complex Selective Population Transfer (SPT) experiments and they have reported values for all of the coupling constants involving ^{31}P nuclei [5]. In the field of platinum–phosphine cluster chemistry it is usually difficult or impossible to determine the signs of the coupling constants but in this case the SPT experiments have revealed relative signs within groups of the coupling constants. These results are shown in Table 4.

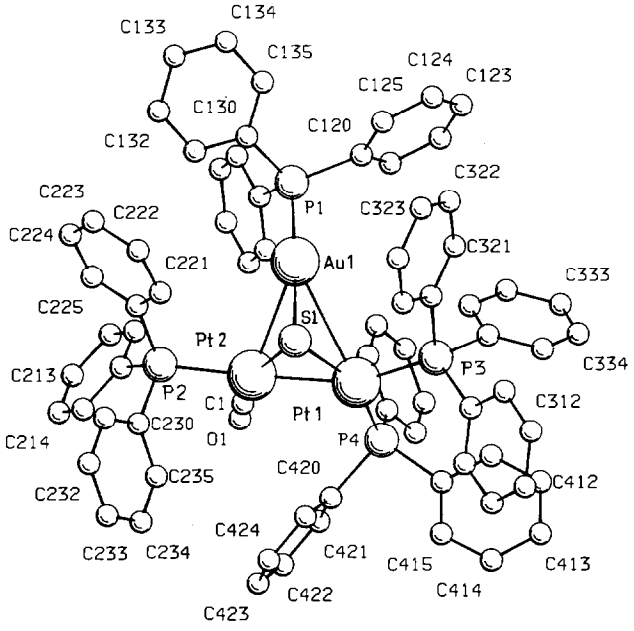

Fig. 1. Molecular geometry of $[Pt_2(\mu\text{-}S)(CO)(PPh_3)_3Au(PPh_3)]^+ PF_6^-$.

The observation of coupling constants with differing signs emphasises the existence of multiple coupling pathways and the care that must be taken in relating magnitudes of one bond coupling constants to bond lengths.

The object of Balch's SPT experiments was to distinguish the spectral lines due to the various isotopomers of the compound so that the coupling constants could be assigned. In this work it has been found that coupling constants can be assigned if the $^{31}P\{^1H\}$ spectrum is examined in conjunction with the $^{195}Pt\{^1H\}$ spectrum. The latter has a reasonably straightforward form owing to the wide separation of the ^{195}Pt chemical shifts and the large values of the $^1J(Pt-P)$ coupling constants. Relative signs of coupling constants can not be assigned by this means, except that computer simulation of the $^{195}Pt\{^1H\}$ spectrum shows up an anomaly in the intensities of some minor lines which may be resolved by correcting $^2J(P(3)-Pt(5))$

TABLE 4

COUPLING CONSTANTS (Hz) FOR $[Pt_2(\mu\text{-}S)(CO)(PPh_3)_3]$ [a]

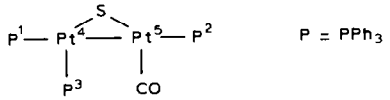

(i)	(ii)	(iii)
$^3J(P(1)-P(2))$ 180	$^1J(P(1)-Pt(4))$ 3462	$^2J(P(1)-Pt(5))$ 280
$^2J(P(1)-P(3))$ −11	$^2J(P(2)-Pt(4))$ 204	$^1J(P(2)-Pt(5))$ 2663
$^3J(P(2)-P(3))$ 22	$^1J(P(3)-Pt(4))$ 3613	$^2J(P(3)-Pt(5))$ −117

[a] Coupling constants within a group have correlated signs.

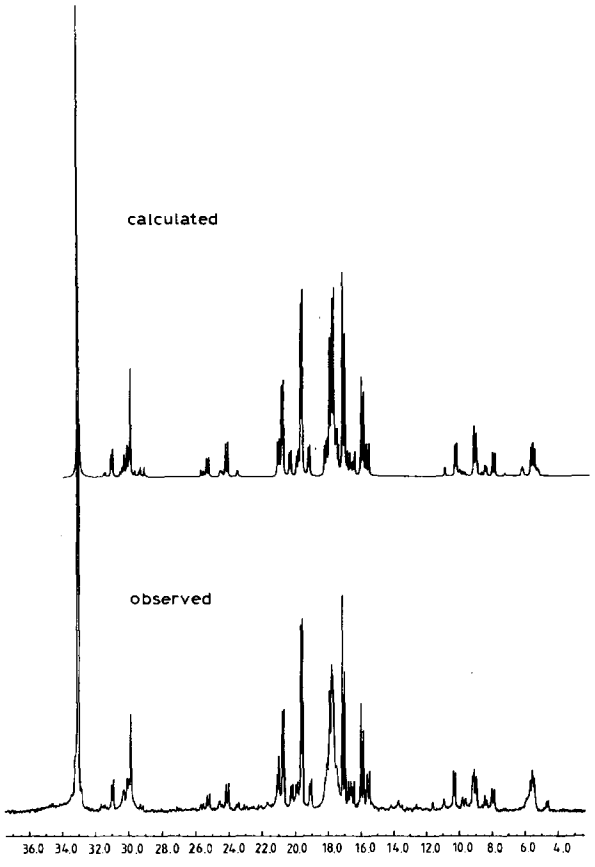

Fig. 2. 162 MHz $^{31}P\{^1H\}$ NMR spectrum of $[Pt_2(\mu\text{-}S)(CO)(PPh_3)_3AuPPh_3]^+$.

(see Table 4) to a negative value. For the purposes of the spectral analysis which follows, advantage has been taken of Balch's SPT results in assigning $^2J(P(3)-Pt(5))$ and $^3J(P(1)-P(3))$ negative values relative to the others.

The parent compound $[Pt_2(\mu\text{-}S)(CO)(PPh_3)_3]$ and the three $[MPR_3]^+$ adducts (**2a–2c**) all give similar $^{31}P\{^1H\}$ and $^{195}Pt\{^1H\}$ NMR spectra. The only significant difference between the compounds is in the signal due to the phosphine of the $[MPR_3]$ fragment. Since the ^{31}P nucleus of this fragment shows no perceptible coupling to platinum, this extra ^{31}P signal affects the form only of the $^{31}P\{^1H\}$ spectra. Examples of the NMR spectra obtained for these compounds are given in Fig. 2 which shows the observed and calculated $^{31}P\{^1H\}$ spectra for $[Pt_2(\mu\text{-}S)(CO)(PPh_3)_3AuPPh_3]^+$, and Fig. 3 which shows the observed and calculated $^{195}Pt\{^1H\}$ spectra for $[Pt_2(\mu\text{-}S)(CO)(PPh_3)_3]$. For compound **2c** (M = Au), the $^{31}P\{^1H\}$ spectrum was recorded at an observation frequency of 162 MHz instead of the usual 101 MHz. This had the effect of spreading out the ^{31}P chemical shifts and so simplifying the spectrum slightly. Consequently it was easier to measure the NMR parameters. The $^{31}P\{^1H\}$ signals for the phosphines of the coordinated MPR_3 fragments are found as very strong singlets in the cases M = Cu ($\delta(^{31}P)$ −3.5 ppm) and M = Au ($\delta(^{31}P)$ 33.1 ppm). For M = Ag, this phosphine is observed

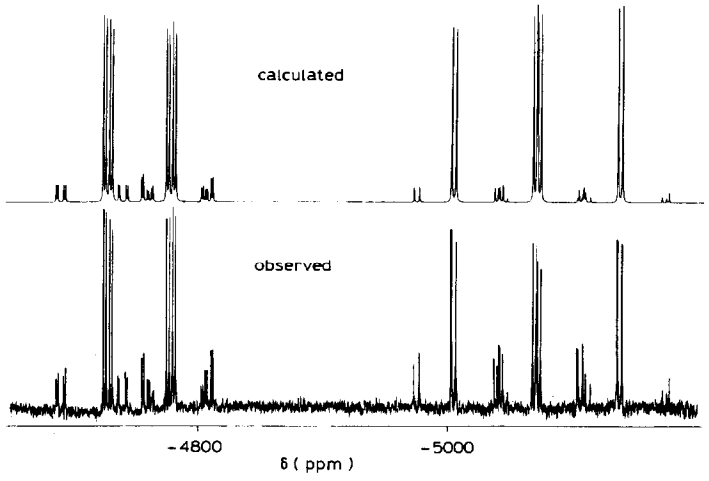

Fig. 3. $^{195}Pt\{^1H\}$ NMR spectrum of $[Pt_2(\mu\text{-}S)(CO)(PPh_3)_3]$.

as a pair of doublets due to slightly different coupling to ^{109}Ag (48%) and ^{107}Ag (52%) (both $I = \frac{1}{2}$). The signals in this case are broad due to the slow relaxation of the silver nuclei (see Fig. 4). The chemical shifts for all of these compounds are given in Table 5 and the coupling constants are collected together in Table 6.

The $^{31}P\{^1H\}$ NMR spectra are very complex and the relative proximity of the chemical shifts for the ^{31}P nuclei attached to the $Pt_2(\mu\text{-}S)$ triangle causes severe second order distortions. Therefore, chemical shifts and coupling constants have to be calculated by iteration from estimates. Good estimates of the coupling constants involving ^{195}Pt nuclei are obtained from the $^{195}Pt\{^1H\}$ NMR spectra which are very much simpler. Since these compounds have only two isotopomers which contain ^{195}Pt, calculation of $^1J(Pt\text{–}Pt)$ is also quite easy.

The ^{195}Pt chemical shifts are consistently to higher field for the platinum which is coordinated to two PPh_3 ligands than for the platinum which is coordinated to PPh_3 and CO ligands, by about 300 ppm in $[Pt_2(\mu\text{-}S)(CO)(PPh_3)_3]$ and by about 200 ppm in the $[MPR_3]^+$ adducts. The ^{31}P chemical shift for the phosphine *cis* to CO is also found to higher field than the other two (by about 4 ppm).

The coupling constants in Table 6 show only small variations between the four compounds except that $^2J(Pt\text{–}P)$ and $^1J(Pt\text{–}Pt)$ are noticeably smaller in the $[MPR_3]^+$ adducts than in the parent compound. The values for the **3–6** coupling are

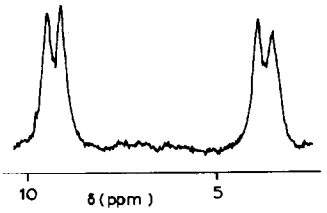

Fig. 4. ^{31}P signals for the $AgPPh_3$ fragment in complex II: $[Pt_2(\mu\text{-}S)(CO)(PPh_3)_3AgPPh_3]^+$.

TABLE 5

^{31}P AND ^{195}Pt CHEMICAL SHIFTS (ppm) FOR $[Pt_2(\mu\text{-}S)(CO)(PPh_3)_3]$ AND ITS $[MPR_3]^+$ ADDUCTS

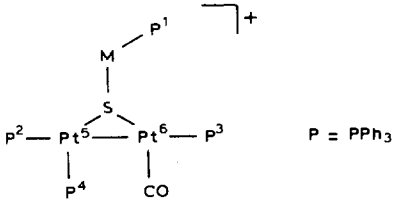

Complex	$\delta(^{31}P)$				$\delta(^{195}Pt)$	
	1	2	3	4	5	6
$[Pt_2(\mu\text{-}S)(CO)(PPh_3)_3]$ (**1**)	–	19.5	15.2	19.1	−5072	−4753
$[Pt_2(\mu\text{-}S)(CO)(PPh_3)_3AuPPh_3]^+$ (**2c**)	33.1	20.1	16.6	17.8	−4841	−4629
$[Pt_2(\mu\text{-}S)(CO)(PPh_3)_3AgPPh_3]^+$ (**2b**)	6.3 [a]	17.7	14.1	16.0	−4857	−4661
$[Pt_2(\mu\text{-}S)(CO)(PPh_3)_3CuPPh_3]^+$ (**2a**)	−3.5	18.6	15.1	16.4	−4864	−4670
$[Pt_2(\mu\text{-}S)(CO)(PPh_3)_3]_2Au^+$ [b] (**3**)	–	22.6	12.6	12.9		

[a] Average of ^{31}P–^{107}Ag and ^{31}P–^{109}Ag. [b] Approximate values.

the smallest encountered in this work for $^1J(Pt-P)$ and are smaller than is found in Pt^0 compounds [11]. This $^1J(Pt-P)$ is for the phosphine which is *cis* to CO and its value being smaller than for the two mutually *cis* phosphines is in agreement with the "*cis* effect" observed by Pregosin [12] in some Pt^{II} complexes. Within each compound, the difference between $^2J(Pt-P)$ for **2–6** and **4–6**, typically +200 and

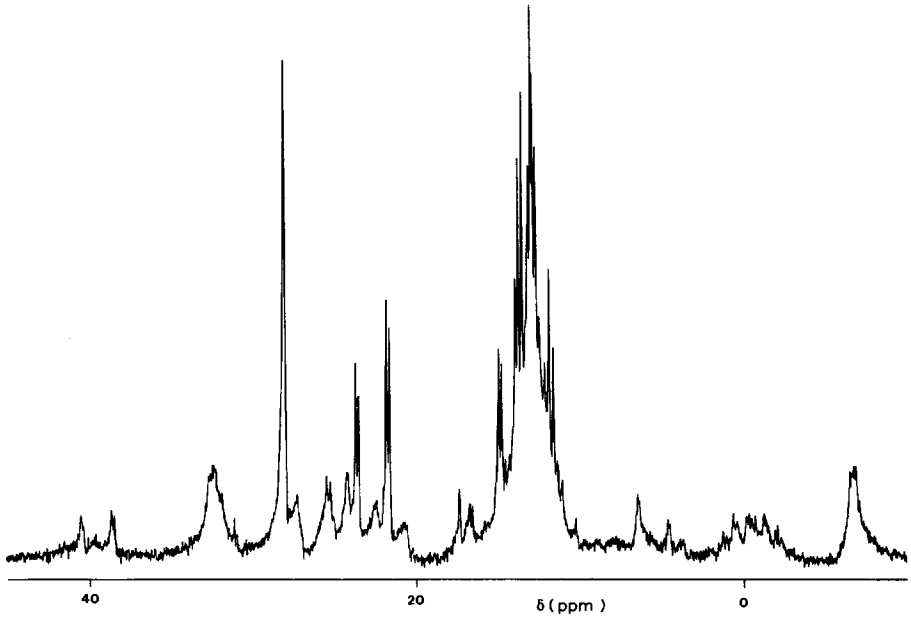

Fig. 5. $^{31}P\{^1H\}$ NMR spectrum of $[Pt_2(\mu\text{-}S)(CO)(PPh_3)_3]_2Au^+$; recorded at −50 °C.

TABLE 6

COUPLING CONSTANTS (Hz) FOR $[Pt_2(\mu\text{-}S)(CO)(PPh_3)_3]$ AND DERIVED COMPOUNDS

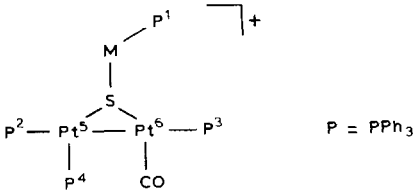

Complex	^1J(Pt–P)			^2J(Pt–P)			^2J(P–P)	^3J(P–P)		^1J(Pt–Pt)
	(2–5)	(4–5)	(3–6)	(2–6)	(4–6)	(3–5)	(2–4)	(3–4)	(2–3)	(5–6)
$[Pt_2(\mu\text{-}S)(CO)(PPh_3)_3]$ (**1**)	3462	3613	2663	280	−117	204	−11	22	180	3628
$[Pt_2(\mu\text{-}S)(CO)(PPh_3)_3AuPPh_3]^+$ (**2c**)	3352	3953	2617	131	−96	148	−17	24	184	2567
$[Pt_2(\mu\text{-}S)(CO)(PPh_3)_3AgPPh_3]^+$ (**2b**) [a]	3299	3832	2586	167	−99	188	−15	23	183	2850
$[Pt_2(\mu\text{-}S)(CO)(PPh_3)_3CuPPh_3]^+$ (**2a**)	3308	3878	2600	150	−98	144	−24	31	182	2630
$[Pt_2(\mu\text{-}S)(CO)(PPh_3)_3]_2Au^+$ (**3**) [b]	3435	3960				160	(−)16	25	192	

[a] Also **2b**: $^1J(^{107}Ag,P)$ and $^1J(^{109}Ag, P)$ one of 615 and one of 536 Hz. [b] Approximate values.

−100 Hz respectively emphasises the need to consider coupling pathways since both values involve the same Pt–Pt bond.

The $^{31}P\{^1H\}$ NMR spectrum at ambient temperature of the complex $[Pt_2(\mu\text{-}S)(CO)(PPh_3)_3]_2Au^+$ gave broad and poorly resolved lines. Therefore, this spectrum was recorded at −50 °C and the result is shown in Fig. 5. Although the lines are still moderately broad and the ^{195}Pt satellites are not well resolved, it is possible to identify the resemblance between this spectrum and that of the parent compound $[Pt_2(\mu\text{-}S)(CO)(PPh_3)_3]$. There is an extra single line at 28.1 ppm which is possibly due to the presence of excess $[AuPPh_3]^+$, but otherwise the spectrum can be interpreted in terms of the same arrangement of ^{31}P and ^{195}Pt nuclei. Some of the NMR parameters were measured approximately and are included in Tables 5 and 6. The coupling constants have similar magnitudes to those of the parent compound but the chemical shifts show a significant change. In $[Pt_2(\mu\text{-}S)(CO)(PPh_3)_3]$, P(2) and P(4) are close together and about 4 ppm to low field of P(3). However, in $[Pt_2(\mu\text{-}S)(CO)(PPh_3)_3]_2Au^+$, P(3) and P(4) are close together and about 10 ppm to high field of P(2). The ^{195}Pt satellites which were sufficiently resolved for coupling constants to be measured are all associated with Pt(5), that is the Pt coordinated to two phosphines.

Experimental

The reactions were routinely carried out using Schlenk-line techniques under pure dry N_2 and using dry oxygen-free solvents. Microanalyses (C, H and N) were carried out by Mr. M. Gascoyne and his staff of this laboratory. Infrared spectra were recorded on a Perkin–Elmer 1710 FT-IR spectrometer as Nujol mulls between KBr discs and calibrated using polystyrene film. Unless otherwise stated, proton decoupled ^{31}P and ^{195}Pt NMR spectra were recorded in deuterated solvents on a Bruker AM250 spectrometer operating at 101.26 and 53.77 MHz respectively. The 162 MHz $^{31}P\{^1H\}$ NMR spectrum of compound **2c** was recorded on the University of London Bruker WH400 spectrometer at Queen Mary College. Chemical shifts were referenced externally to aqueous solutions of trimethylphosphate and Na_2PtCl_6 respectively. Chemical shifts were taken as positive to high frequency of the reference. Computer simulations of the NMR spectra were carried out using a program developed by Prof. R.K. Harris, then of the University of East Anglia, and adopted for use on the Oxford University VAX system by Dr. A.E. Derome.

X-Ray crystallographic analysis

The geometric diffraction data were collected on an Enraf–Nonius CAD4 diffractometer in the $\omega/2\theta$ scan mode with θ scan width of 0.9°, using graphite-monochromated Mo-K_α (λ 0.71069 Å) radiation. Problems with crystal decomposition limited the overall accuracy of the data set. 3522 unique, absorption corrected reflections out of 6478 measured in the range 1–25° had $I \geqslant 3\sigma(I)$ and were used to solve the structure by standard Fourier and Patterson methods.

The structure was refined using blocked matrix least-squares techniques with the platinum, gold, phosphorus and sulphur atoms refined with anisotropic thermal parameters and the remainder isotropically.

The phenyl rings were constrained to idealised geometries with the exception of the gold–phosphine moiety for which there was difficulty in locating all the carbon

atoms. This resulted either from a rotational disorder associated with this phosphine ligand, or the relative quality of the data resulting from the decomposition of the crystal in the X-ray beam.

Residual peaks of 3 $eÅ^{-3}$ were found associated with two of the inversion centres and were modelled as disordered CH_2Cl_2 molecules with half occupancies for the carbon atoms. The final difference Fourier map showed four peaks of approximately 2 $eÅ^{-3}$ in an empty region of the unit cell, but these could not be satisfactorily modelled either in terms of CH_2Cl_2 or Et_2O molecules of crystallisation.

A Chebyshev weighting scheme gave satisfactory agreement analyses with the following coefficients: 245.4, 328.1 and 128.1 [13–15].

Synthesis of $[Pt_2(\mu\text{-}S)(CO)(PPh_3)_3]$

This compound was prepared by a modification of the method of Balch et al. [5]. $Pt(PPh_3)_3$ (6.0 g, 4.9 mmol) was suspended in pentane (40 cm^3). COS gas was bubbled through for about 20 min until the suspension was almost white. The solid was then filtered off and dissolved in the minimum volume of $CHCl_3$. Pentane was added to precipitate a yellow powder which was then suspended in ethanol and refluxed under nitrogen. A bright yellow solid, $[Pt_2(\mu\text{-}S)(CO)(PPh_3)_3] \cdot \frac{1}{2}PhH$, was filtered off and dried in vacuo. Yield 3.5 g (90%). Elemental analysis: Found: C, 54.6; H, 4.0. $C_{58}H_{48}OP_3Pt_2S$ calc: C, 54.6; H, 3.8%. Infra-red spectrum (cm^{-1}): ν(CO) 2001s. $^{31}P\{^1H\}$ NMR in CD_2Cl_2 solution: $\delta(^{31}P)$ 15.2, 19.1, 19.5 ppm (Ref. 5 18.7, 23.1, 23.3 ppm from H_3PO_4); $\delta(^{195}Pt)$ −5072, −4753 ppm. Crystals for X-ray diffraction were grown by slow diffusion of diethyl ether into an acetone solution.

Synthesis of $[Pt_2(\mu\text{-}S)(CO)(PPh_3)_3Au(PPh_3)]^+ PF_6^-$

To a solution of $[Pt_2(\mu\text{-}S)(CO)(PPh_3)_3]$ (0.17 g, 0.14 mmol) in THF (30 cm^3) were added, with stirring, $[Au(PPh_3)Cl]$ (0.07 g, 0.14 mmol) and $TlPF_6$ (0.05 g, 0.14 mmol). After 6 h the solvent was removed in vacuo and the residue extracted into CH_2Cl_2. Addition of diethyl ether to the filtered solution gave, on standing, yellow needle-like crystals of $[Pt_2(\mu\text{-}S)(CO)(PPh_3)_3Au(PPh_3)]^+ PF_6^-$. Yield: 0.21 g (83%). Elemental analysis: Found: C, 47.2; H, 3.7. $C_{73}H_{60}AuF_6OP_5Pt_2S$ calc: C, 47.6; H, 3.3%. Infra-red spectrum (cm^{-1}): ν(CO) 2025s; $\nu(PF_6)$ 838s. NMR in CD_2Cl_2 solution: $\delta(^{31}P)$ 33.1, 20.1, 17.8, 16.6 ppm; $\delta(^{195}Pt)$ −4841, −4629 ppm. Single crystals for X-ray diffraction were grown by slow diffusion of diethyl ether into a CH_2Cl_2 solution.

Synthesis of $[Pt_2(\mu\text{-}S)(CO)(PPh_3)_3Ag(PPh_3)]^+ PF_6^-$

$[Pt_2(\mu\text{-}S)(CO)(PPh_3)_3Ag(PPh_3)]^+ PF_6^-$ was prepared by the same method as the Au analogue (see above), using $[Ag(PPh_3)Cl]_4$ in four-fold excess and allowing 3 d for the reaction to be complete. Quantities used were: $[Pt_2(\mu\text{-}S)(CO)(PPh_3)_3]$ (0.13 g, 0.11 mmol), $[Ag(PPh_3)Cl]_4$ (0.18 g, 0.11 mmol) and $TlPF_6$ (0.19 g, 0.54 mmol) in THF (25 cm^3). The product was recrystallised from CH_2Cl_2/hexane. Yield: 0.13 g (71%). Elemental analysis: Found: C, 49.9; H, 3.0; Ag, 6.6. $C_{73}H_{60}AgF_6OP_5Pt_2S$ calc: C, 50.0; H, 3.4; Ag, 6.2. Infra-red spectrum (cm^{-1}): ν(CO) 2022s; $\nu(PF_6)$ 835s. $^{31}P\{^1H\}$ NMR in CD_2Cl_2 solution: $\delta(^{31}P)$ 6.3, 17.7, 16.0, 14.1 ppm; $\delta(^{195}Pt)$ −4857, −4661 ppm.

Synthesis of $[Pt_2(\mu\text{-}S)(CO)(PPh_3)_3Cu(PPh_3)]^+ PF_6^-$

The procedure described in Ref. 1 (Section 6.4.3) was used, with the following reagents: $[Pt_2(\mu\text{-}S)(CO)(PPh_3)_3]$ (0.27 g, 0.22 mmol), $[Cu(PPh_3)Cl_4]$ (0.08 g, 0.06 mmol) and $TlPF_6$ (0.08 g, 0.23 mmol) in THF (25 cm^3). The product was obtained as pale yellow crystals from CH_2Cl_2/diethyl ether. Yield: 0.31 g (83%). Elemental analysis: Found C, 51.0; H, 3.5. $C_{73}H_{60}CuF_6OP_5Pt_2S$ calc: C, 51.3; H, 3.5%. Infra-red spectrum (cm^{-1}): ν(CO) 2016s. NMR in CD_2Cl_2 solution: $\delta(^{31}P)$ −3.4, 18.6, 16.4 15.1 ppm; $\delta(^{195}Pt)$ −4864, −4670 ppm.

Synthesis of $[Pt_2(\mu\text{-}S)(CO)(PPh_3)_3]_2Au^+ PF_6^-$

$[Pt_2(\mu\text{-}S)(CO)(PPh_3)_3]$ (0.22 g, 0.18 mmol) was dissolved in benzene (30 cm^3) and $TlPF_6$ (0.07 g, 0.20 mmol) added with stirring followed by $[Au(Me_2S)Cl]$ (0.03 g, 0.10 mmol). The mixture was stirred for 1 h during which time the solution became colourless and an orange solid was precipitated. This product was filtered off, washed with a little benzene and then extracted into CH_2Cl_2. Addition of hexane gave, on standing overnight at −20 °C, orange microcrystals of $[Pt_2(\mu\text{-}S)(CO)(PPh_3)_3]_2Au^+ PF_6^-$. Yield: 0.21 g (84%). Elemental analysis: Found: C, 47.2; H, 3.6; Au, 6.5; Pt, 26.4%. $C_{110}H_{90}AuF_6O_2P_7Pt_4S_2$ calc: C, 46.9; H, 3.2; Au, 7.0; Pt, 27.7%. Infra-red spectrum (cm^{-1}): ν(CO) 2031s, 2019s; $\nu(PF_6)$ 839s. $^{31}P\{^1H\}$ NMR in CD_2Cl_2 solution: $\delta(^{31}P)$ 22.6, 12.9, 12.6 ppm.

Acknowledgement

The S.E.R.C. is thanked for financial support, Johnson-Matthey Ltd. for a generous loan of platinum and gold metals and Dr. Martin Grossel for obtaining the 162 MHz NMR spectrum described in the paper.

References

1 Part VI. D.I. Gilmour, M.A. Luke and D.M.P. Mingos, J. Chem. Soc., Dalton. Trans., in press and references therein.
2 M.C. Baird and G. Wilkinson, J. Chem. Soc. (A), (1967) 865.
3 M.C. Baird and G. Wilkinson, J. Chem. Soc., Chem. Commun., (1966) 514.
4 A.C. Skapski and P.G.H. Troughton, J. Chem. Soc. (A), (1969) 2772.
5 C.T. Hunt, G.B. Matson and A.L. Balch, Inorg. Chem., 20 (1981) 2270.
6 C.E. Briant, D.I. Gilmour and D.M.P. Mingos, J. Chem. Soc., Dalton Trans., (1986) 835.
7 D.M.P. Mingos and R.W.M. Wardle, J. Chem. Soc., Dalton Trans., (1986) 73.
8 C.E. Briant, R.W.M. Wardle and D.M.P. Mingos, J. Organomet. Chem., 267 (1984) C49.
9 P.G. Jones, G.M. Sheldrick and E. Hädicke, Acta Crystallogr., B36 (1980) 2777.
10 P.G. Jones, Gold. Bull., 14 (1981) 102; 14 (1981) 159.
11 J. Chatt, R. Mason and D.W. Meek, J. Amer. Chem. Soc., 97 (1975) 3826.
12 P.S. Pregosin, R. Favez, R. Roulet, T. Boshi, A. Michelin and R. Ros, Inorg. Chim. Acta, 45 (1980) L7.
13 J.R. Carruthers, CRYSTALS User Manual, Oxford University Computing Centre, 1975.
14 K. Davies, CHEMFRAG User Manual, Chemical Crystallography Laboratory, Oxford, 1981.
15 International Tables of X-ray Crystallography, Kynoch Press, Birmingham, 1974, Vol. 4, p. 99.